Chapter 4

Study of Other Physical Observables

Other physical observables like forward-backward asymmetry $A_{FB}^{\ell}(q^2)$, longitudinal $P_L^{\ell}(q^2)$, transverse $P_T^{\ell}(q^2)$ polarization of the charged leptons, lepton side convexity parameter C_F^{ℓ} and longitudinal polarization fraction for the final vector meson $F_L(q^2)$ play an extremely important role in order to study the effect of lepton mass in semileptonic decays because these observables are dependent of lepton mass. These observables also provide more detailed physical picture of semileptonic decay beyond the branching fraction study. These physical observables are not yet reported by any experimental facilities worldwide. These physical observables are identified experimentally for the other semileptonic decays at B factories, however, they are yet to be reported for the channels studied here. These observables are also extremely sensitive and useful for testing the lepton flavor violating decays and thus can serve as probes for the physics beyond the standard model.

4.1 Other Physical Observable for $b \to (c,u)\ell\nu_\ell$ transition

4.1.1 Forward-Backward Asymmetry

Let's first consider the forward-backward asymmetry. $\theta \in [0, \pi/2]$ and $\theta \in [\pi/2, \pi]$ are the requirements for forward and backward region respectively. Hence $A^\ell_{FB}(q^2)$ is defined as,

$$A^\ell_{FB}(q^2) = \frac{3}{4}\Big[\frac{H_P - 4\delta_\ell H_{SL}}{H_{tot}}\Big] \tag{4.1}$$

4.1.2 Longitudinal And Transverse Polarization

The longitudinal polarization $P^\ell_L(q^2)$ is defined as the ratio of polarized decay distribution to the unpolarized decay distribution [225] and is given by

$$\begin{aligned} P^\ell_L(q^2) &= \frac{(1-\delta_\ell)|H_n|^2 - 3\delta_\ell|H_t|^2}{(1+\delta_\ell)|H_n|^2 + 3\delta_\ell|H_t|^2} \\ &= \frac{(H_U + H_L)(1-\delta_\ell) - 3\delta_\ell H_S}{H_{tot}} \end{aligned} \tag{4.2}$$

Similarly the definition of transverse polarization $P^\ell_T(q^2)$ in which the direction of leptonic polarization is perpendicular to its momentum direction is given by

$$P^\ell_T = -\frac{3\pi\sqrt{\delta_\ell}}{4\sqrt{2}}\frac{H_P + 2H_{SL}}{H_{tot}} \tag{4.3}$$

4.1.3 Leptonic Convexity Parameter

The leptonic convexity parameter is defined as the second derivative of normalized angular distribution with respect to $(\cos\theta)^2$. The normalized angular distribution of

θ is defined in [225] as

$$\tilde{W}(\theta) = \frac{W(\theta)}{H_{tot}} = \frac{a + b\cos\theta + c\cos\theta}{2(a + c/3)}$$

where

$$\begin{aligned} a &= 3/8 \times [(1 + 2\delta_\ell)H_U + 2H_L + 4\delta_\ell H_S] \\ b &= 3/8 \times (2H_P - 8\delta_\ell H_{SL}) \\ c &= 3/8 \times [(1 - 2\delta_\ell)H_U - 2(1 - 2\delta_\ell)H_S] \end{aligned}$$

and now using above definition leptonic convexity parameter is defined as

$$C_F^\ell(q^2) = \frac{d^2\tilde{W}(\theta)}{d(\cos\theta)^2} = \frac{c}{a + c/3} = \frac{3}{4}(1 - 2\delta_\ell)\frac{H_U - 2H_L}{H_{tot}} \tag{4.4}$$

4.1.4 Longitudinal And Transverse Polarization Fraction

The longitudinal polarization fraction of the final vector meson is given by

$$F_L(q^2) = \frac{(1 + \delta_\ell)H_L + 3\delta_\ell H_S}{H_{tot}} \tag{4.5}$$

Transverse polarization fraction of the final vector meson can also be obtained via relation $F_T = 1 - F_L$.

In all the above Eq. (4.1) $-$ (4.5), δ_ℓ is known as helicity flip factor and is given by $\delta_\ell = \frac{m_l^2}{2q^2}$ and $H's$ are bilinear combinations of helicity components related to hadronic tensor related to helicity structure functions and given as [209, 226, 227]

$$\begin{aligned} H_U &= |H_+|^2 + |H_-|^2, \quad H_P = |H_+|^2 - |H_-|^2 \\ H_L &= |H_0|^2, \quad H_S = |H_t|^2, \quad H_{SL} = Re(H_0 H_t^\dagger). \end{aligned}$$

For $M_1 \to M_2$ transitions, H_t,$H_\pm$ and H_0 is given by Eq. (3.12) whereas for $M_1 \to M_2^{(*)}$ transitions, H_t, $H_\pm$ and H_0 is given by equation Eq. (3.13).

The average value of these observables has been calculated by multiplying them with the phase factor $C(q^2) = |\boldsymbol{P}_2|(q^2 - m_\ell^2)/q^2$ both in the numerator and denominator and then integrated separately. Illustratively,

$$\langle A_{FB}^{\ell} \rangle \;=\; \frac{3}{4} \frac{\int dq^2 C(q^2)(H_P - 4\delta_\ell H_{SL})}{\int dq^2 C(q^2) H_{tot}} \tag{4.6}$$

same process is performed for all other observables also to obtain their average value. For all the observables defined above Eq. (4.1) − (4.6), H_{tot} is given by Eq. (3.26).

4.1.5 Results and Discussion

The average values of other observables for $B_s \to D_s^{(*)-}$ and $B_s \to K^{(*)-}$ transitions are listed in Tab. 4.1. The results are plotted in Fig. 4.1 − 4.10. It is important to note here that these parameters are calculated for entire physical range of momentum transfer.

4.2 Other Physical Observable for $b \to d\ell^+\ell^-$ transition

4.2.1 Forward-Backward Asymmetry

Here the forward-backward asymmetry is given as

$$A_{\rm FB}^{\ell} = \frac{3}{4}\beta_\ell \frac{\mathcal{H}_P^{12}}{\mathcal{H}_{\rm tot}}. \tag{4.7}$$

Table 4.1: Other Observable Parameters for $B_s \to (K^{(*)-}, D_s^{(*)-})$ transitions

Channel	A_{FB}	P_L	P_T	C_F	F_L
$B_s \to Ke^+\nu_e$	-3.936×10^{-7}	1	-0.007	-1.500	- - -
$B_s \to K\mu^+\nu_\mu$	-0.006	0.987	-0.121	-1.481	- - -
$B_s \to K\tau^+\nu_\tau$	-0.280	0.166	-0.846	-0.635	- - -
$B_s \to D_s e^+\nu_e$	-1.160×10^{-6}	-1.000	0.001	-1.500	- - -
$B_s \to D_s\mu^+\nu_\mu$	-0.015	-0.958	0.205	-1.455	- - -
$B_s \to D_s\tau^+\nu_\tau$	-0.362	0.179	0.839	-0.260	- - -
$B_s \to K^* e^+\nu_e$	-0.371	1	-0.000	-0.218	0.430
$B_s \to K^*\mu^+\nu_\mu$	-0.373	0.994	-0.022	-0.212	0.430
$B_s \to K^*\tau^+\nu_\tau$	-0.424	0.628	-0.027	-0.030	0.417
$B_s \to D_s^* e^+\nu_e$	0.195	-1.000	-0.0003	-0.452	0.534
$B_s \to D_s^*\mu^+\nu_\mu$	0.190	-0.985	-0.057	-0.436	0.534
$B_s \to D_s^*\tau^+\nu_\tau$	0.029	-0.515	-0.126	-0.060	0.458

4.2.2 Longitudinal and Transverse Polarization

The longitudinal and transverse polarization is given as

$$F_L = \frac{1}{2}\beta_\ell^2 \frac{\mathcal{H}_L^{11} + \mathcal{H}_L^{22}}{\mathcal{H}_{\rm tot}}, \qquad F_T = \frac{1}{2}\beta_\ell^2 \frac{\mathcal{H}_U^{11} + \mathcal{H}_U^{22}}{\mathcal{H}_{\rm tot}}. \tag{4.8}$$

θ in Eq. (4.7) is the polar angle between momentum transfer($\overrightarrow{q} = \overrightarrow{p_1} - \overrightarrow{p_2}$) and momentum of parent meson ($\overrightarrow{k_1}$) in the $\ell^+\ell^-$ rest frame.

4.2.3 Clean Observables

Clean observables are given by

$$\begin{aligned}
\langle P_1\rangle_{\rm bin} &= -2\,\frac{\int_{\rm bin} dq^2\,\beta_\ell^2\,[\mathcal{H}_T^{11}+\mathcal{H}_T^{22}]}{\int_{\rm bin} dq^2\,\beta_\ell^2\,[\mathcal{H}_U^{11}+\mathcal{H}_U^{22}]},\\
\langle P_2\rangle_{\rm bin} &= -\,\frac{\int_{\rm bin} dq^2\,\beta_\ell\,\mathcal{H}_P^{12}}{\int_{\rm bin} dq^2\,\beta_\ell^2\,[\mathcal{H}_U^{11}+\mathcal{H}_U^{22}]},\\
\langle P_3\rangle_{\rm bin} &= -\,\frac{\int_{\rm bin} dq^2\,\beta_\ell^2\,[\mathcal{H}_{IT}^{11}+\mathcal{H}_{IT}^{22}]}{\int_{\rm bin} dq^2\,\beta_\ell^2\,[\mathcal{H}_U^{11}+\mathcal{H}_U^{22}]},\\
\langle P_4'\rangle_{\rm bin} &= 2\,\frac{\int_{\rm bin} dq^2\,\beta_\ell^2\,[\mathcal{H}_I^{11}+\mathcal{H}_I^{22}]}{N_{\rm bin}},\\
\langle P_5'\rangle_{\rm bin} &= -2\,\frac{\int_{\rm bin} dq^2\,\beta_\ell\,[\mathcal{H}_A^{12}+\mathcal{H}_A^{21}]}{N_{\rm bin}},\\
\langle P_6'\rangle_{\rm bin} &= -2\,\frac{\int_{\rm bin} dq^2\,\beta_\ell\,[\mathcal{H}_{II}^{12}+\mathcal{H}_{II}^{21}]}{N_{\rm bin}},\\
\langle P_8'\rangle_{\rm bin} &= 2\,\frac{\int_{\rm bin} dq^2\,\beta_\ell^2\,[\mathcal{H}_{IA}^{11}+\mathcal{H}_{IA}^{22}]}{N_{\rm bin}},
\end{aligned} \tag{4.9}$$

The helicity structure functions in the above equation are defined as [223],

$$\begin{aligned}
&\mathcal{H}_U^{ij} = {\rm Re}\Big(H^i_{+1+1}H^{\dagger j}_{+1+1}\Big) + {\rm Re}\Big(H^i_{-1-1}H^{\dagger j}_{-1-1}\Big), \quad \mathcal{H}_T^{ij} = {\rm Re}\Big(H^i_{+1+1}H^{\dagger j}_{-1-1}\Big)\\
&\mathcal{H}_P^{ij} = {\rm Re}\Big(H^i_{+1+1}H^{\dagger j}_{+1+1}\Big) - {\rm Re}\Big(H^i_{-1-1}H^{\dagger j}_{-1-1}\Big), \quad \mathcal{H}_{IT}^{ij} = {\rm Im}\Big(H^i_{+1+1}H^{\dagger j}_{-1-1}\Big)\\
&\mathcal{H}_I^{ij} = \frac{1}{2}\Big[{\rm Re}\Big(H^i_{+1+1}H^{\dagger j}_{00}\Big) + {\rm Re}\Big(H^i_{-1-1}H^{\dagger j}_{00}\Big)\Big]\\
&\mathcal{H}_A^{ij} = \frac{1}{2}\Big[{\rm Re}\Big(H^i_{+1+1}H^{\dagger j}_{00}\Big) - {\rm Re}\Big(H^i_{-1-1}H^{\dagger j}_{00}\Big)\Big]\\
&\mathcal{H}_{II}^{ij} = \frac{1}{2}\Big[{\rm Im}\Big(H^i_{+1+1}H^{\dagger j}_{00}\Big) + {\rm Im}\Big(H^i_{-1-1}H^{\dagger j}_{00}\Big)\Big]\\
&\mathcal{H}_I^{ij} = \frac{1}{2}\Big[{\rm Im}\Big(H^i_{+1+1}H^{\dagger j}_{00}\Big) - {\rm Im}\Big(H^i_{-1-1}H^{\dagger j}_{00}\Big)\Big]
\end{aligned}$$

Here $N_{\rm bin}$ is the normalization factor defined as

$$\mathcal{N}_{\rm bin} = \sqrt{\int_{\rm bin} dq^2\,\beta_\ell^2\,[\mathcal{H}_U^{11}+\mathcal{H}_U^{22}]\cdot\int_{\rm bin} dq^2\,\beta_\ell^2\,[\mathcal{H}_L^{11}+\mathcal{H}_L^{22}]}. \tag{4.10}$$

The CP-averaged angular observables $S_{3,4}$ are given as [223]

$$S_3 = \frac{1}{2}F_T P_1 \quad S_4 = \frac{1}{2}\sqrt{F_T F_L}P_4' \tag{4.11}$$

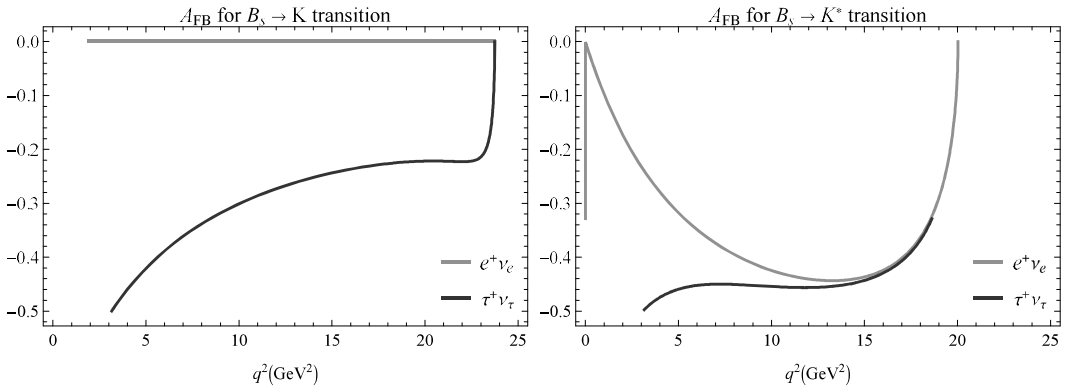

Figure 4.1: Forward-Backward Asymmetry for $B_s \to K^{(*)-}$ transitions

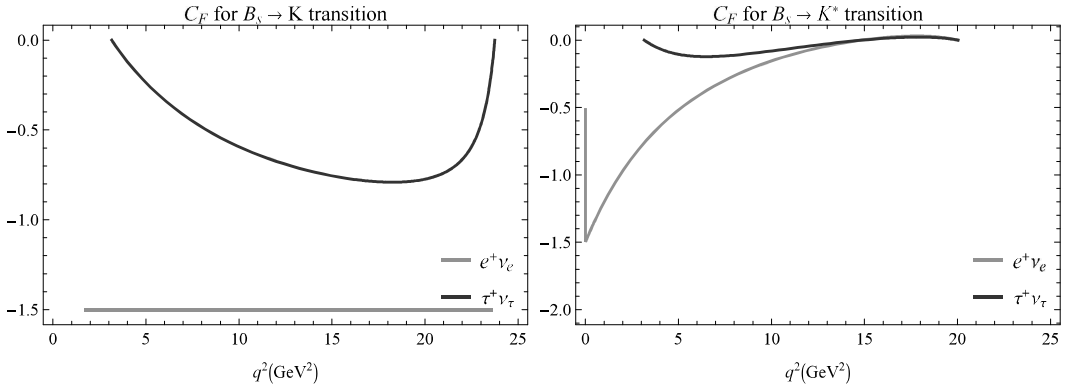

Figure 4.2: Convexity parameters for $B_s \to K^{(*)-}$ transitions

4.2.4 Results and Discussion

Using the calculated form factors in previous chapter we have calculated the other observables parameters like decay widths, forward backward asymmetry and polarization of daughter mesons for rare $b \to d$ transition. As mentioned in previous chapter, these observables are crucial to understand the physics beyond standard model (SM) because they help us to understand how different flavor of leptons behave in the final stage of decay product, which is described here in terms of angular distribution between the charged lepton pairs and momentum of daughter meson. The details of the computation technique used to calculate these observables are adopted from [126,223], where these parameters are calculated for rare decay of B_c meson. All the observables calculated here are described in terms of helicity structure functions and form factors.

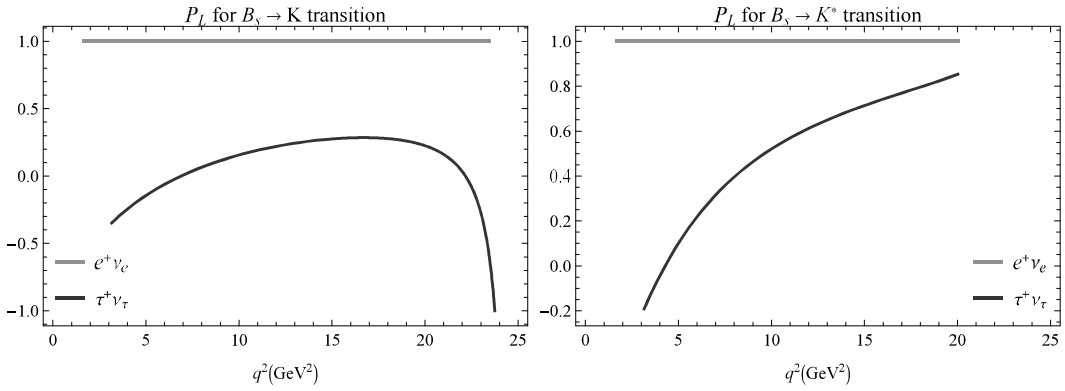

Figure 4.3: Longitudinal polarization for $B_s \to K^{(*)-}$ transitions

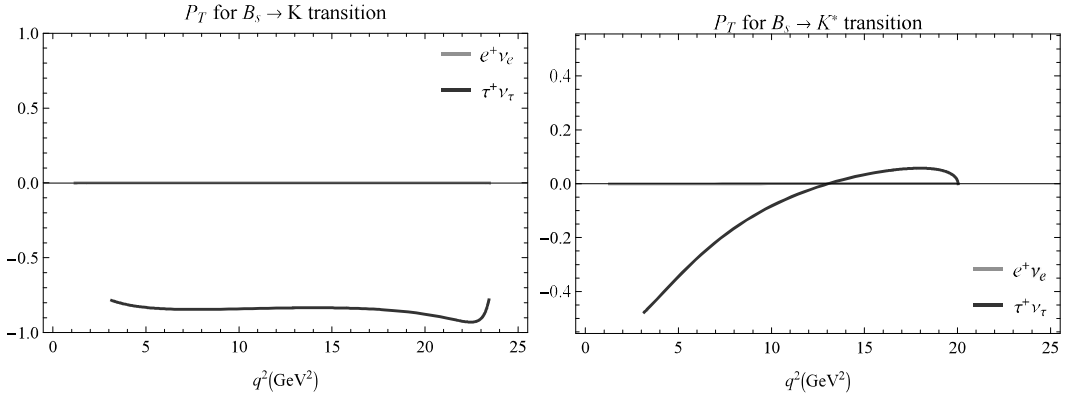

Figure 4.4: Transverse polarization for $B_s \to K^{(*)-}$ transitions

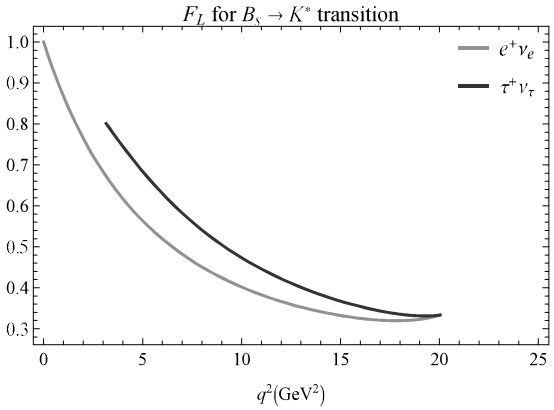

Figure 4.5: Longitudinal Polarization Fraction for $B_s \to K^*$ transition

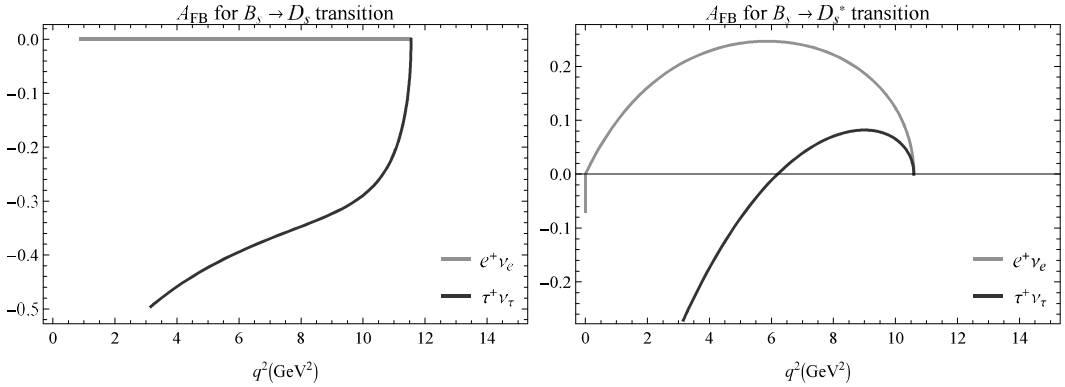

Figure 4.6: Forward-Backward Asymmetry for $B_s \to D_s^{(*)-}$ transitions

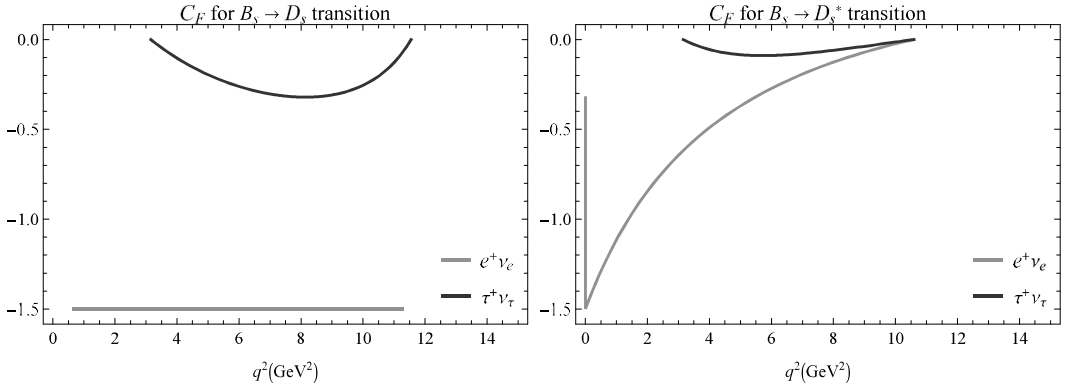

Figure 4.7: Convexity parameters for $B_s \to D_s^{(*)-}$ transitions

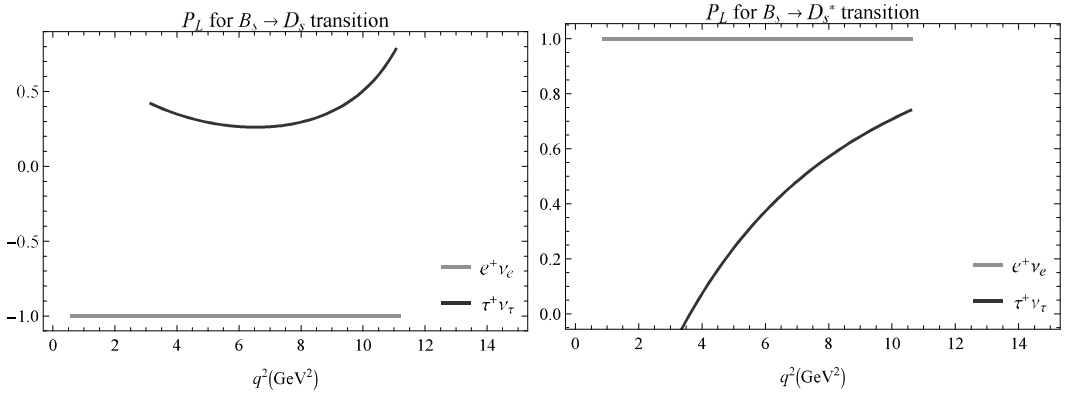

Figure 4.8: Longitudinal polarization for $B_s \to D_s^{(*)-}$ transitions

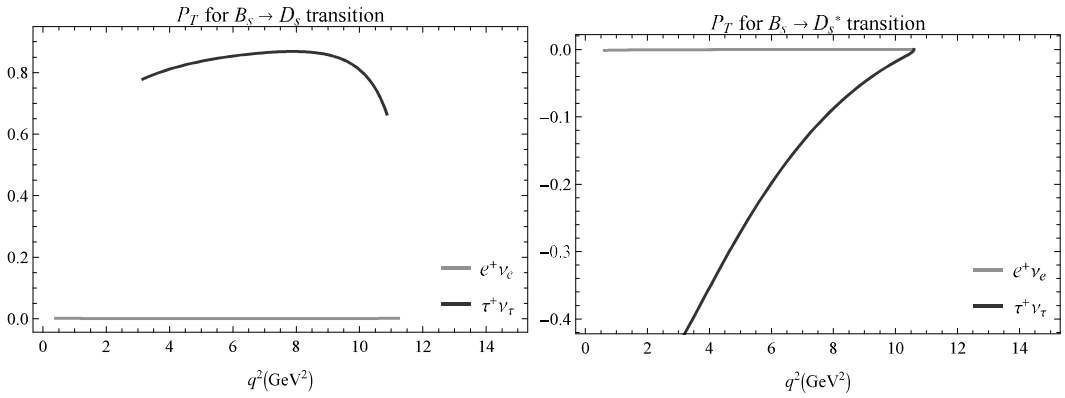

Figure 4.9: Transverse polarization for $B_s \to D_s^{(*)-}$ transitions

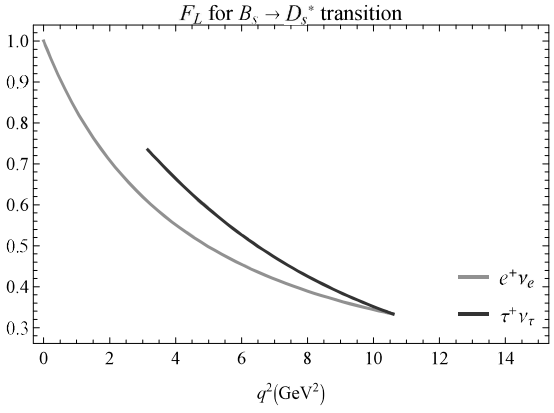

Figure 4.10: Longitudinal Polarization Fraction for $B_s \to D_s^*$ transition

In Fig. 4.11, forward-backward asymmetry, longitudinal polarization and transverse polarization are plotted in the whole q^2 range keeping in mind both resonant and non-resonant contributions. For computing the resonant contribution of these observables, the experimental vetoed regions corresponding to vector resonances are excluded.

For further computations of clean observables, the helicity amplitudes corresponding to form factors are also utilised [228]. These observables have already been reported by LHCb [229,230] and Belle [231] collaboration for $b \to s$ rare decay and hence these are also expected for the $b \to d$ decays. These observables P_i are computed using the relations expressed in Refs. [223, 232]. The plots for the clean observables $P_{1,2,3}$ and $P'_{4,5,8}$ for the channels $B^+ \to \rho^+$ and $B_s^0 \to \bar{K}^*(892)^0$ are displayed in Fig. 4.12 − 4.13. Similar plots can also obtained for the $B^0 \to (\rho^0, \omega)$ transitions. Only muon and tau modes are presented in all plots for observables. It is important to note that the plots for electron mode fully overlaps with that of the muon mode. The average values of these observables considering resonance contributions for transition corresponding to $B^+ \to \rho^+$, $B^0 \to (\rho^0, \omega)$ to $B_s^0 \to \bar{K}^*(892)^0$ channels are also listed in Tab. 4.2 − 4.3. Note that in Tab. 4.2 − 4.3, the sum of longitudinal and transverse polarizations are different than 1 as the leptons have finite mass in present calculations as opposed to case of massless leptons where it would be unity. The same has been explicitly studied in [228,233]. Wilson coefficients which are obtained at the next-to-leading logarithmic order are used in our calculation of the observables in the full kinematical region of the momentum transfer squared. At this order, the coefficient $C_9^{\rm eff}$ takes an imaginary part. The optimized observable P'_6 is identically zero at this order due to the fact that our form factors are real. Further, inspired by pQCD [14] and LCSR [234] point of views, all the physical observables are also computed in the low q^2 bins: [0.1 – 0.98] GeV^2 and [1.1 – 6] GeV^2 corresponding to dropping the charm resonances for electron and muon channels along with the comparison in Tab. 4.4 - 4.6. It is to be noted that the uncertainties in the calculations of form factor has propagated to the computations of branching fractions and other physical observables and this is the only source of uncertainty in the calculations of branching fractions and other physical observables. Higher uncertainties are observed in very low q^2 range, whereas the maximum propagated uncertainty in the branching fractions is about 49 % for all the channel $B^{+(0)} \to \rho^{+(0)} e^+ e^-$ when integrated for the entire q^2 range.

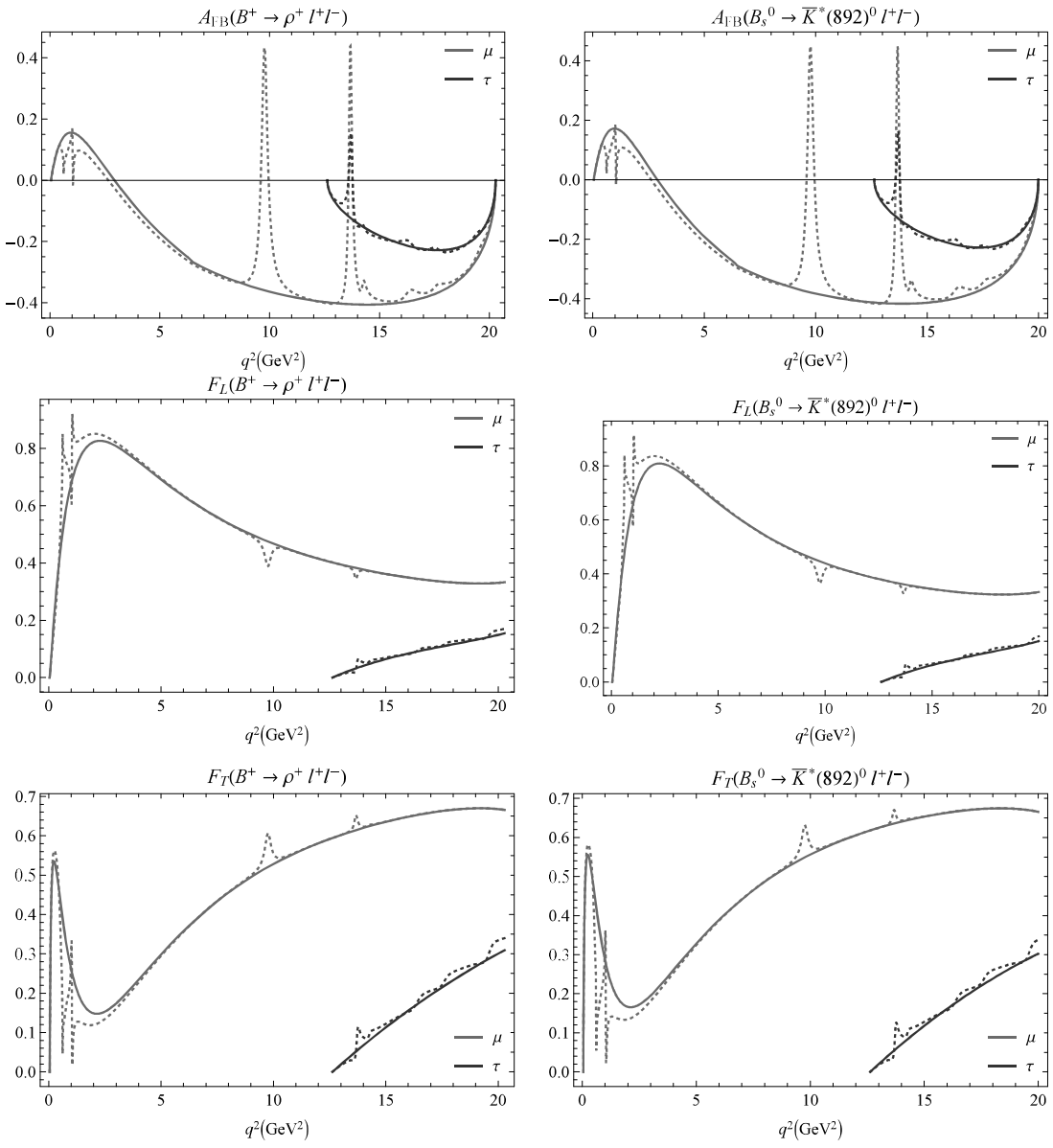

Figure 4.11: Forward backward asymmetry, longitudinal and transverse polarizations (solid lines - excluding resonances, dashed lines - including vector resonances).

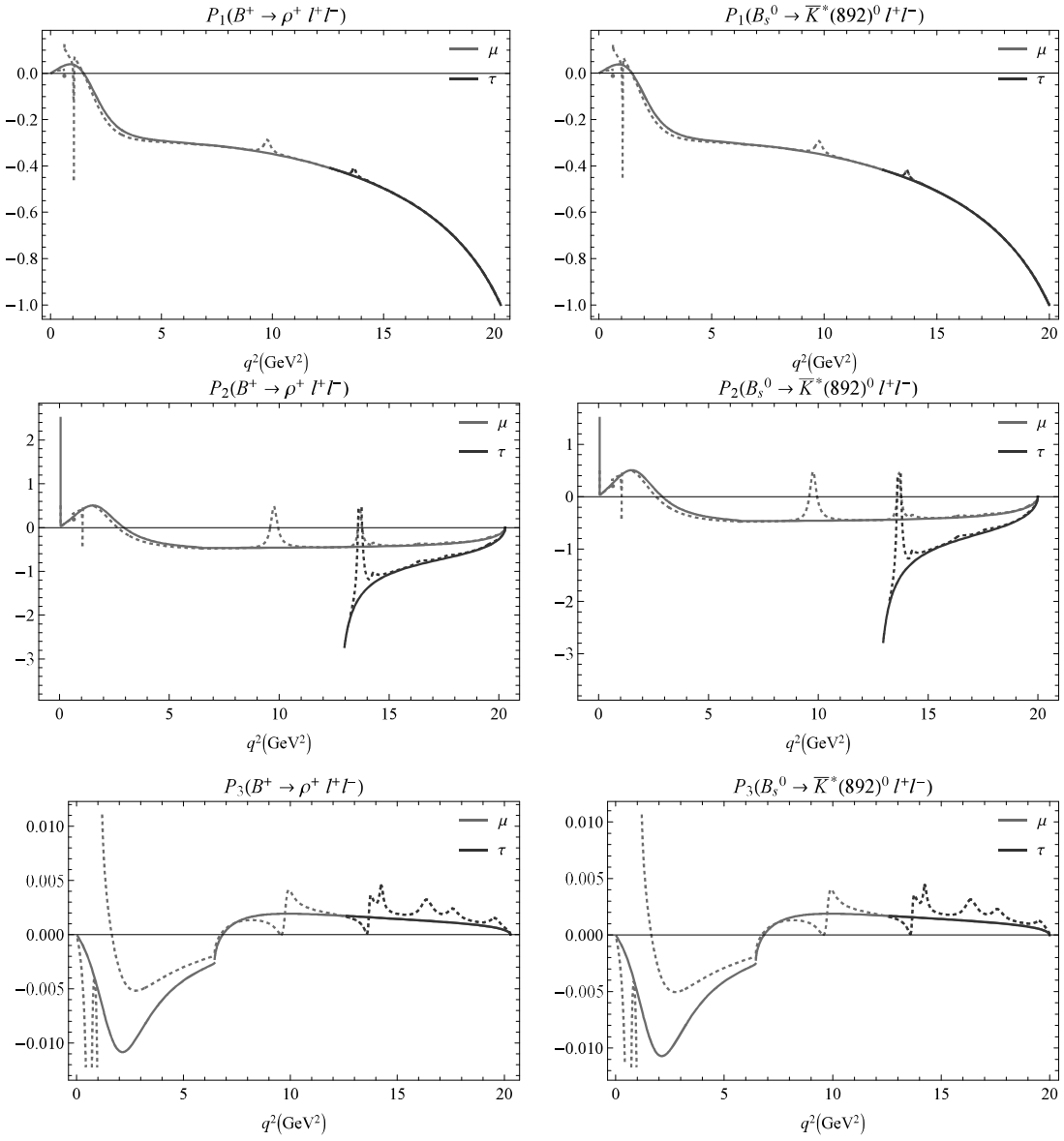

Figure 4.12: Clean observables $P_{1,2,3}$ in whole q^2 range (solid lines - excluding resonances, dashed lines - including vector resonances).

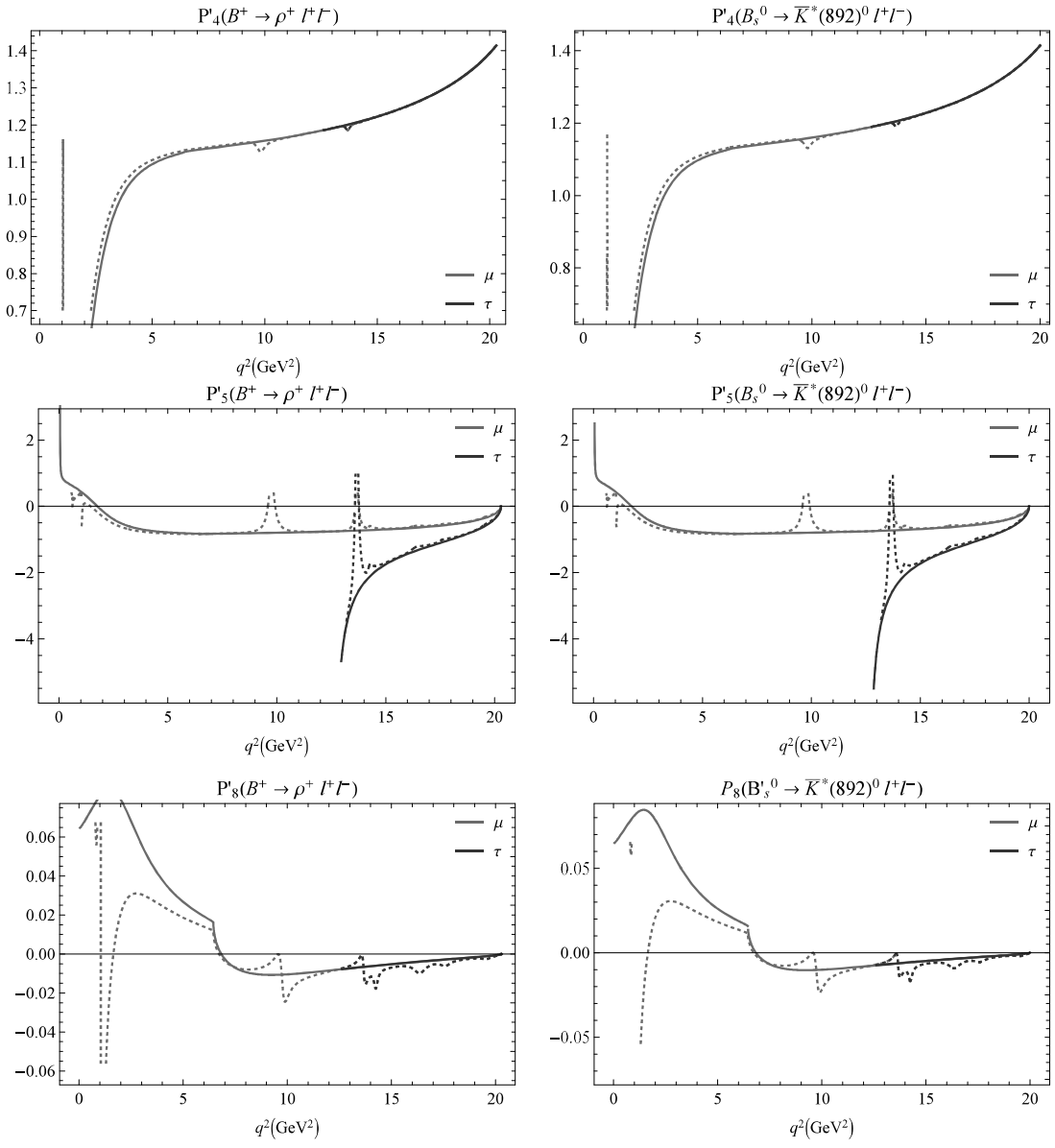

Figure 4.13: Clean observables $P'_{4,5,8}$ in whole q^2 range (solid lines - excluding resonances, dashed lines - including vector resonances).

Table 4.2: q^2- averages of polarization observables over the whole allowed kinematic region for $B^+ \to \rho^+\ell^+\ell^-$, $B^0 \to \rho^0\ell^+\ell^-$ channels

Obs.	$B^+ \to \rho^+\ell^+\ell^-$			$B^0 \to \rho^0\ell^+\ell^-$		
	e^+e^-	$\mu^+\mu^-$	$\tau^+\tau^-$	e^+e^-	$\mu^+\mu^-$	$\tau^+\tau^-$
$-\langle A_{FB}\rangle$	0.178	0.226	0.207	0.179	0.227	0.209
$\langle F_L\rangle$	0.417	0.510	0.110	0.414	0.506	0.110
$\langle F_T\rangle$	0.563	0.455	0.217	0.567	0.458	0.218
$-\langle P_1\rangle$	0.297	0.460	0.688	0.294	0.457	0.686
$-\langle P_2\rangle$	0.211	0.331	0.636	0.211	0.331	0.637
$10^4 \times \langle P_3\rangle$	0.326	2.198	17.694	-1.422	-0.518	13.063
$\langle P_4'\rangle$	0.735	0.993	1.297	0.738	0.994	1.296
$-\langle P_5'\rangle$	0.385	0.543	1.000	0.384	0.543	1.002
$10^2 \times \langle P_8'\rangle$	3.058	2.741	-0.468	3.112	2.802	-0.372
$-\langle S_3\rangle$	0.083	0.105	0.074	0.083	0.105	0.075
$\langle S_4\rangle$	0.178	0.239	0.100	0.179	0.239	0.101

Table 4.3: q^2- averages of polarization observables over the whole allowed kinematic region for $B^0 \to \omega \ell^+ \ell^-$ and $B_s^0 \to \bar{K}^*(892)^0 \ell^+ \ell^-$ channels

Obs.	$B^0 \to \omega \ell^+ \ell^-$			$B_s^0 \to \bar{K}^*(892) \ell^+ \ell^-$		
	e^+e^-	$\mu^+\mu^-$	$\tau^+\tau^-$	e^+e^-	$\mu^+\mu^-$	$\tau^+\tau^-$
$-\langle A_{FB} \rangle$	0.184	0.229	0.203	0.194	0.244	0.207
$\langle F_L \rangle$	0.415	0.501	0.111	0.394	0.479	0.107
$\langle F_T \rangle$	0.566	0.465	0.218	0.588	0.488	0.218
$-\langle P_1 \rangle$	0.322	0.486	0.706	0.317	0.475	0.701
$-\langle P_2 \rangle$	0.216	0.328	0.620	0.220	0.333	0.631
$10^4 \times \langle P_3 \rangle$	0.526	2.498	17.584	0.930	2.934	17.175
$\langle P_4' \rangle$	0.768	1.017	1.304	0.776	1.019	1.303
$-\langle P_5' \rangle$	0.388	0.537	0.970	0.401	0.549	0.985
$10^2 \times \langle P_8' \rangle$	2.905	2.559	-0.447	2.826	2.475	-0.440
$-\langle S_3 \rangle$	0.091	0.113	0.077	0.093	0.116	0.077
$\langle S_4 \rangle$	0.186	0.246	0.102	0.186	0.246	0.100

Table 4.4: Value of other observables at different bin values for $B \to \rho \ell^+ \ell^-$ channel where, $\ell = e$ and μ

Obs.	q^2	$B \to \rho e^+ e^-$		$B \to \rho \mu^+ \mu^-$		
		$B^+ \to \rho^+$	$B^0 \to \rho^0$	$B^+ \to \rho^+$	$B^0 \to \rho^0$	LCSR [234]
$10^9 \times \mathcal{B}$	$[0.1, 0.98]$	2.58 ± 2.18	1.19 ± 0.98	2.54 ± 2.15	1.17 ± 0.97	2.165 ± 0.302
	$[1.1, 6]$	7.51 ± 4.52	3.42 ± 2.07	7.49 ± 4.52	3.41 ± 2.07	4.064 ± 0.778
$\langle A_{FB} \rangle$	$[0.1, 0.98]$	0.089	0.090	0.079	0.080	-0.046 ± 0.005
	$[1.1, 6]$	-0.085	-0.085	-0.085	-0.085	-0.024 ± 0.018
$\langle R_\rho \rangle$	$[0.1, 0.98]$	0.984	0.983	0.984	0.983	0.955 ± 0.194
	$[1.1, 6]$	0.997	0.997	0.997	0.997	1.036 ± 0.289
$\langle F_L^\rho \rangle$	$[0.1, 0.98]$	0.511	0.506	0.447	0.443	0.409 ± 0.067
	$[1.1, 6]$	0.779	0.776	0.763	0.761	0.822 ± 0.039
$\langle P_1 \rangle$	$[0.1, 0.98]$	0.017	0.016	0.019	0.018	0.050 ± 0.181
	$[1.1, 6]$	-0.254	-0.252	-0.255	-0.253	-0.044 ± 0.110
$\langle P_2 \rangle$	$[0.1, 0.98]$	0.122	0.121	0.146	0.146	0.083 ± 0.010
	$[1.1, 6]$	-0.256	-0.254	-0.259	-0.257	0.074 ± 0.053
$\langle P_3 \rangle$	$[0.1, 0.98]$	-0.008	-0.008	-0.009	-0.009	-0.228 ± 0.044
	$[1.1, 6]$	-0.003	-0.003	-0.003	-0.003	-0.229 ± 0.028
$\langle P_4' \rangle$	$[0.1, 0.98]$	-0.291	-0.282	-0.288	-0.279	-0.591 ± 0.077
	$[1.1, 6]$	0.878	0.879	0.882	0.883	0.470 ± 0.161
$\langle P_5' \rangle$	$[0.1, 0.98]$	0.447	0.453	0.468	0.474	0.368 ± 0.043
	$[1.1, 6]$	-0.625	-0.622	-0.632	-0.628	-0.178 ± 0.084
$\langle P_8' \rangle$	$[0.1, 0.98]$	0.312	0.313	0.321	0.322	-0.133 ± 0.021
	$[1.1, 6]$	0.014	0.014	0.014	0.014	0.113 ± 0.013

Table 4.5: Value of other observables at different bin values for $B^0 \to \omega\ell^+\ell^-$ channel where, $\ell = e$ and μ

Obs.	q^2	$B^0 \to \omega e^+e^-$	$B^0 \to \omega\mu^+\mu^-$	Obs.	q^2	$B^0 \to \omega e^+e^-$	$B^0 \to \omega\mu^+\mu^-$
$10^9 \times \mathcal{B}$	$[0.1, 0.98]$	0.94 ± 0.80	0.92 ± 0.78	$\langle P_2 \rangle$	$[0.1, 0.98]$	0.123	0.147
	$[1.1, 6]$	2.78 ± 1.67	2.77 ± 1.66		$[1.1, 6]$	-0.259	-0.263
$\langle A_{FB} \rangle$	$[0.1, 0.98]$	0.090	0.080	$\langle P_3 \rangle$	$[0.1, 0.98]$	-0.009	-0.010
	$[1.1, 6]$	-0.088	-0.087		$[1.1, 6]$	-0.003	-0.003
$\langle R_\omega \rangle$	$[0.1, 0.98]$	0.979	0.979	$\langle P_4' \rangle$	$[0.1, 0.98]$	-0.286	-0.282
	$[1.1, 6]$	0.996	0.996		$[1.1, 6]$	0.894	0.898
$\langle F_L^\omega \rangle$	$[0.1, 0.98]$	0.511	0.447	$\langle P_5' \rangle$	$[0.1, 0.98]$	0.447	0.469
	$[1.1, 6]$	0.774	0.759		$[1.1, 6]$	-0.618	-0.625
$\langle P_1 \rangle$	$[0.1, 0.98]$	0.018	0.021	$\langle P_8' \rangle$	$[0.1, 0.98]$	0.312	0.321
	$[1.1, 6]$	-0.273	-0.274		$[1.1, 6]$	0.014	0.014

Table 4.6: Value of other observables at different bin values for $B_s^0 \to \bar{K}^*(892)^0 \ell^+ \ell^-$ channel where, $\ell = e$ and μ

Obs.	q^2	$B_s^0 \to \bar{K}^*(892)^0 e^+ e^-$		$B_s^0 \to \bar{K}^*(892)^0 \mu^+ \mu^-$		
		Present	pQCD [14]	Present	pQCD [14]	LCSR [234]
$10^9 \times \mathcal{B}$	$[0.1, 0.98]$	1.89 ± 1.25	$1.63^{+0.65}_{-0.43}$	1.86 ± 1.23	$1.60^{+0.64}_{-0.42}$	$3.812 \pm 0.450 \pm 0.086$
	$[1.1, 6]$	5.54 ± 2.73	$5.22^{+2.13}_{-1.59}$	5.51 ± 2.72	$5.21^{+2.12}_{-1.58}$	$7.803 \pm 1.758 \pm 0.357$
$\langle A_{FB} \rangle$	$[0.1, 0.98]$	0.096	0.096 (2)	0.085	0.085 (2)	$-0.060 \pm 0.008 \pm 0.001$
	$[1.1, 6]$	-0.099	$-0.064(3)$	-0.098	$-0.064(3)$	$-0.029 \pm 0.020 \pm 0.009$
$\langle R_{K^*} \rangle$	$[0.1, 0.98]$	0.984	0.984 (1)	0.984	0.984 (1)	$0.940 \pm 0.009 \pm 0.001$
	$[1.1, 6]$	0.995	0.997 (1)	0.995	0.997 (1)	$0.998 \pm 0.004 \pm 0.0$
$\langle F_L^{K^*} \rangle$	$[0.1, 0.98]$	0.479	0.442 (8)	0.420	0.446 (8)	$0.453 \pm 0.067 \pm 0.014$
	$[1.1, 6]$	0.752	0.780 (10)	0.738	0.783 (10)	$0.853 \pm 0.038 \pm 0.007$
$\langle P_1 \rangle$	$[0.1, 0.98]$	0.016	0.110 (2)	0.019	0.012 (2)	$0.012 \pm 0.129 \pm 0.001$
	$[1.1, 6]$	-0.257	$-0.306(30)$	-0.258	$-0.307(30)$	$-0.081 \pm 0.111 \pm 0.005$
$\langle P_2 \rangle$	$[0.1, 0.98]$	0.123	0.115 (1)	0.147	0.129 (1)	$0.118 \pm 0.013 \pm 0.001$
	$[1.1, 6]$	-0.266	$-0.193(10)$	0.270	$-0.196(10)$	$0.112 \pm 0.072 \pm 0.036$
$\langle P_3 \rangle$	$[0.1, 0.98]$	-0.008	0.005 (1)	-0.009	0.005 (1)	$0.001 \pm 0.002 \pm 0.0$
	$[1.1, 6]$	-0.003	0.002 (1)	-0.003	0.002 (1)	$0.004 \pm 0.010 \pm 0.002$
$\langle P_4' \rangle$	$[0.1, 0.98]$	-0.284	$-0.369(3)$	-0.280	$-0.365(3)$	$-0.593 \pm 0.057 \pm 0.009$
	$[1.1, 6]$	0.890	0.895 (10)	0.894	0.899 (10)	$0.464 \pm 0.164 \pm 0.014$
$\langle P_5' \rangle$	$[0.1, 0.98]$	0.445	0.541 (1)	0.466	0.512 (1)	$0.547 \pm 0.051 \pm 0.016$
	$[1.1, 6]$	-0.634	$-0.575(40)$	-0.641	$-0.578(40)$	$-0.286 \pm 0.125 \pm 0.046$
$\langle P_8' \rangle$	$[0.1, 0.98]$	0.313	0.396 (1)	0.322	0.399 (1)	$0.015 \pm 0.003 \pm 0.016$
	$[1.1, 6]$	0.014	0.006 (1)	0.014	0.006 (1)	$0.040 \pm 0.004 \pm 0.017$